Photoresponse in Self-Assembled Films of Carbon Nanotubes

Yumeng Shi,[†] Dongliang Fu,[†] Dan H. Marsh,*[,‡] Graham A. Rance,[‡] Andrei N. Khlobystov, and Lain-Jong Li*[,†]

School of Materials Science and Engineering, Nanyang Technological University 50, Nanyang Avenue, Singapore, 639798, Singapore, and School of Chemistry, University of Nottingham, University Park, Nottingham, NG7 2RD, United Kingdom

Received: April 22, 2008; Revised Manuscript Received: June 4, 2008

Water-soluble single-walled carbon nanotubes (SWNT; with carboxylic functionalities) were self-assembled on a water−pentane interface. Ultrathin (<30 nm) films consisting of two distinct types of nanotube morphologies, wide bundles of nanotubes interwoven with a network of thin bundled (or individual) tubes, were obtained. The films were highly homogeneous and sufficiently robust to be transferred from the liquid interface and deposited onto solid substrates such as silica, quartz, or plastic. Under normal conditions the electrical conductance of such films is metal-like and is dominated by the transport of charge carriers through bundles of SWNT. However, semiconducting SWNT within the structure can readily accept charge carriers (holes) from excitons generated in optically active conjugated polymers upon absorption of visible light. This increase in concentration of charge carriers stimulated by light in interfacial SWNT−polymer films results in a measurable conductance change that depends linearly on the applied voltage and the intensity of light when the light intensity is low. Critically, neither drop-cast SWNT samples nor interfacial films of multiwalled carbon nanotube (MWNT) exhibit any photoresponsive behavior and thus the photoresponse of the SWNT−polymer composite depends on the morphology of the nanotubes and their assembly methodology.

Introduction

Single-walled carbon nanotubes (SWNT) are promising electronic materials for a variety of applications such as field-effect transistors (FET),[1,2] memory devices,[3,4] and chemical/biological sensors.[5] Studies on SWNT networks[6–17] demonstrate that such devices could be assembled by using more practical fabrication methods. If the novel properties of these reported nanodevices were incorporated in micro- or macroscale devices then fabrication costs would be effectively lowered. Traditional device assembly methods often include drop-cast assemblies of SWNT. Given the poorly controlled nature of the deposition processes during drop-casting, the resulting films are thick and inhomogeneous relative to thin films deposited by other techniques such as spin-coating. Herein we discuss the incorporation of an interfacially assembled, ultrathin, 2-dimensional (2D) nanotube network into an active device. A key advantage of such dimensionally confined structures is the efficient deposition of a continuous conductive assembly of nanotubes, minimizing the mass of material used and maximizing the functional surface area accessible in the final device. By thus optimizing the interaction area of the device it is more likely that the novel and attractive electronic properties of SWNT may be harnessed for optoelectronic or sensing applications.

Recently the photoconductivity of semiconducting-SWNT has been attributed to direct excitation through their van Hove interband transitions.[18–22] The photocurrent was due to photon-induced exciton generation and subsequent charge separation by an electric field. The role of metal electrodes on the photoconductivity of nanotubes through the modulation of Schottky barrier height has also been proposed.[20,23–27] The observation of photoconductivity was sometimes complicated by a decrease in conductance, which was ascribed to photoinduced oxygen desorption from the surface of nanotubes[28,29] or the surface oxide layer at the contacts.[30,31] Optoelectronic switching behavior due to interaction between photosensitive dyes/polymers and SWNT transistors has been proposed to serve in memory devices[32,33] and photoactivated charge transfer has been observed in C_{60} encapsulated in SWNT.[34] It was reported that photogenerated holes were transferred to nanotubes, resulting in a current increase.[32] An alternative mechanism, "photoinduced electrostatic gating" has also been proposed.[33] This states that photocurrents are due to the trapping of photogenerated electrons at SiO_2 dielectric surfaces, which then effectively gate the transistor. Although different mechanisms have been suggested, these experiments indicated that semiconducting nanotubes in the ensemble were playing dominant roles in photoconductivity of these species. In addition, photons were directly absorbed by the polymers and therefore the devices could be tuned to respond to the desired wavelength by choosing appropriate photosensitive polymers. Optoelectronic studies of large-area 2D layers of carbon nanotubes are vital for constructing smart structures with multiple functionalities. It has been suggested that macroscale, multifunctional carbon nanotube ensembles are essential in the fields of photodetection, flat and flexible displays, and flexible solar cells, which are able to cover nonflat surfaces.[17,27] Here we report on an interfacial assembly method[35] to form ultrathin, pseudomonolayer networks of SWNT or multiwalled carbon nanotube (MWNT) networks from surfactantless solutions of nanotubes,[36] where the uniform web-like nanotube structures can cover hundreds of square microns in area.[35] We specifically investigate photoresponsive behavior in these structures. This behavior is compared to that for drop-cast SWNT films (dc-SWNT) and differences are discussed in terms of their respective structure.

* Corresponding author. E-mail: ljli@ntu.edu.sg; dan.marsh@nottingham.ac.uk.
[†] Nanyang Technological University 50.
[‡] University of Nottingham.

10.1021/jp803477t CCC: $40.75
Published on Web 07/30/2008

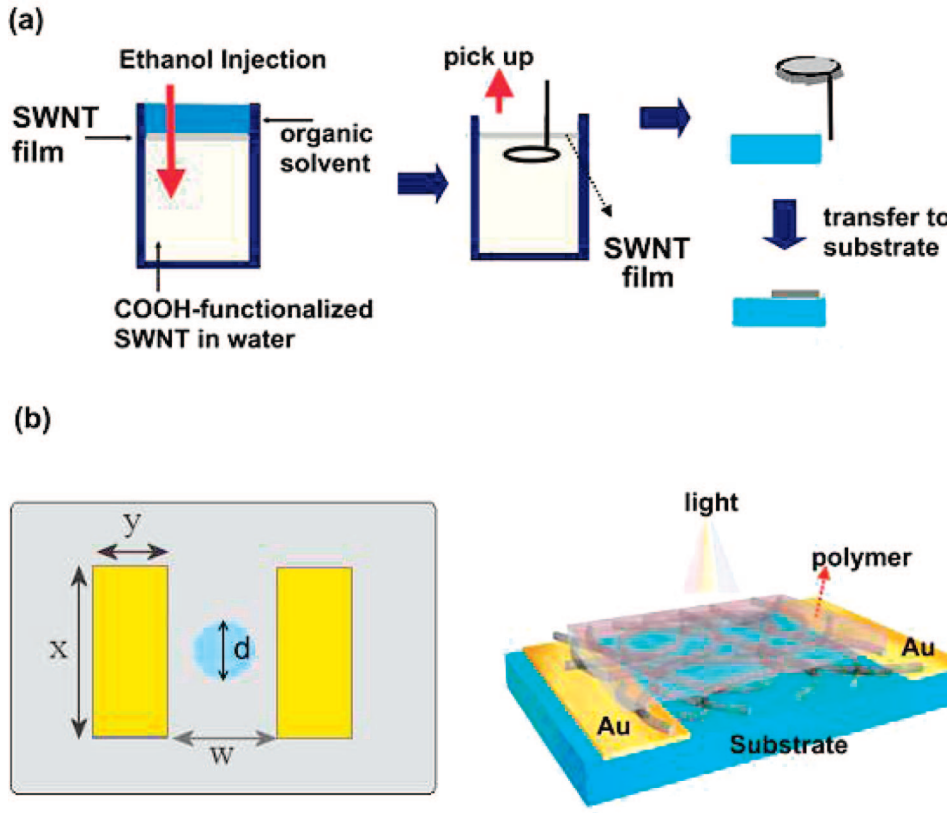

Figure 1. (a) Schematic illustration showing the preparation of interfacial films of single-walled carbon nanotubes on substrates. Ethanol is an antisolvent that speeds up the formation of the interfacial SWNT films. (b) Diagram and cartoon of device geometry; x, channel width (electrode length) = 1 mm; y, electrode width = 1 mm; w, channel length (electrode separation) = 125 μm; and d, the diameter of the illumination spot = 75 μm.

Experimental Section

Carboxylic acid functionalized SWNT (~4 to 6 atomic % of COOH) were produced by arc-discharge and purchased from Carbon Solutions, Inc. (USA). Catalytic chemical vapor deposition synthesized thin MWNTs (~4 atomic % of COOH) with an average diameter of 10 nm were purchased from Nanocyl. Carboxylic group functionalized SWNT or MWNT aqueous solutions (2.5 mL, 0.01 mg mL^{-1}) were added to a 10 mL glass vial. Anhydrous pentane (1 mL) was carefully layered onto the surface to create an interface between the organic and aqueous phases. An antisolvent, ethanol (1 mL), was then rapidly injected through the organic layer to precipitate carbon nanotubes at the interface. A cap is needed to cover the vial for a few minutes to minimize evaporation-induced convective motion of the interface. The interfacial film is rapidly formed and visible at the interface within minutes. After the evaporation of the organic phase, a floating film is left on the surface of the aqueous solution. The film was transfer-printed onto quartz substrates, rinsed with deionized water (>18.2 MΩ·cm), and blown dry with nitrogen. Drop-cast SWNT or MWNT films were prepared by direct casting of the COOH-functionalized SWNT or COOH-functionalized MWNT on to quartz substrates and left to dry under ambient conditions. The prepared SWNT or MWNT films were around 80−100 nm thick on average for photoconductivity study and ~300−400 nm thick for sheet resistance measurements. The polymer poly[(9,9-dioctylfluorenyl-2,7-diyl)-co-(bithiophene)] (F8T2) was purchased from American Dye Source and used without further purification. The photosensitive polymer F8T2 (with an average thickness of ~100 nm determined by surface profilometry) was deposited on top of the devices by spin coating from a toluene solution (4 mg·mL^{-1}).

All electrical measurements were performed under ambient conditions with a Keithley semiconductor parameter analyzer, model 4200-SCS. The thickness of polymer films was characterized with an α-step IQ surface profiler manufactured by KLA Tencor. Sheet resistance was measured with a CMT-SR 2000N 4-point probe station from Advanced Instrument Technology. Incident light of desired wavelengths was selected by the use of band-pass filters (±10 nm) from a broadband light source (450 W short arc Xe lamp, or 250 W tungsten lamp). Incident power intensity was calibrated for each wavelength or sample measured to ensure comparability. The power intensity of light was measured by a commercially available Si-photodiode.

Results and Discussion

Figure 1a schematically shows the method by which interfacial SWNT films (i-SWNT) are formed and transferred to substrates. A free-standing film of COOH-functionalized SWNT was formed on a water−pentane interface. After evaporation of the superphase, a floating film is left on the surface of the aqueous solution and can, in a way analogous to Langmuir−Blodgett (LB) films, be sampled from the surface though dip-coating. In this study, a more controllable method is used whereby the floating, LB-like film is captured from the air/water interface by using a flame-cleaned Pt specimen loop and transferred to the desired substrate.

The network resistor devices were fabricated in a device geometry shown in Figure 1b (which includes electrode dimensions), where i-SWNT films were transferred onto prepatterned gold electrodes on quartz wafers. The morphology of the i-SWNT films was assessed by AFM (Figure 2a,b) and TEM (Figure 2c,d). It can be seen from these images that continuous

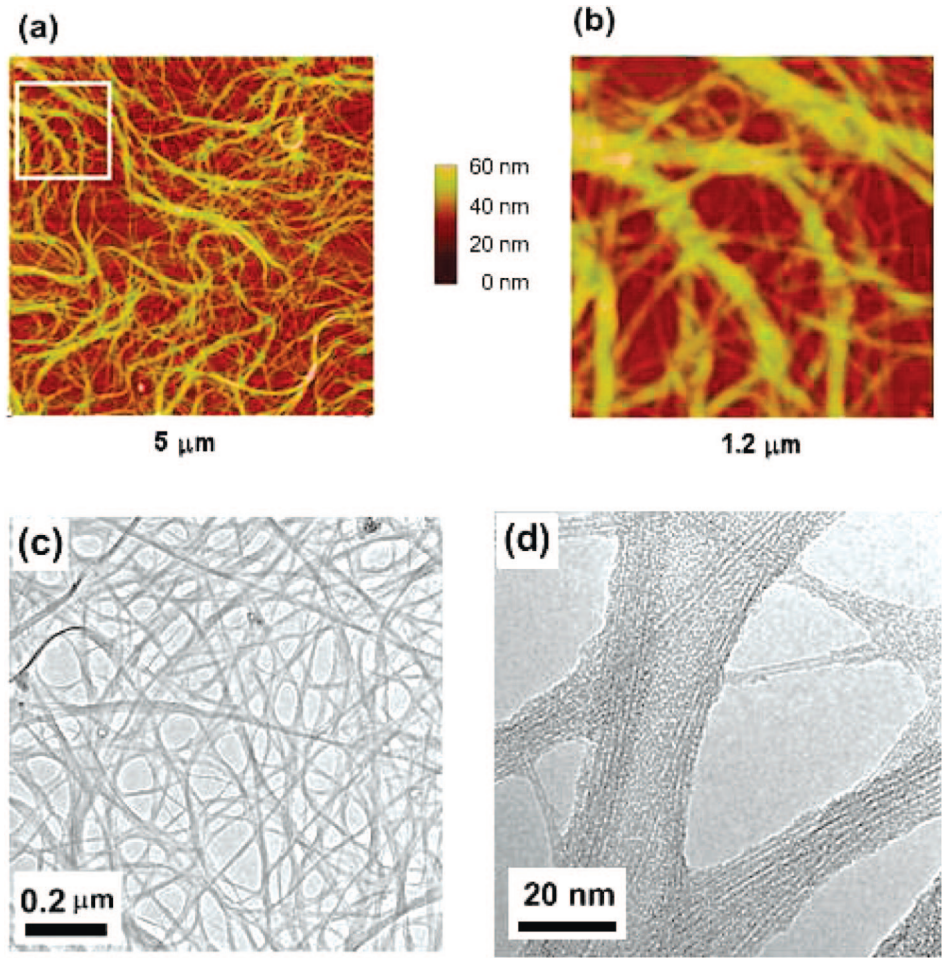

Figure 2. Morphology of the i-SWNT film: (a) AFM image of the i-SWNT network on a quartz wafer and (b) enlarged selected area of panel a showing that thin nanotubes are interwoven with thick bundled tubes. Film thickness can be deduced from the *z*-scale. (c) TEM image of the i-SWNT film with (d) a higher resolution image showing the mixture of discrete and bundled nanotubes.

networks of i-SWNT uniformly cover an area of several hundreds of square micron. The networks are very thin (<30 nm, determined from the *z*-scale on the AFM images between the substrate and the film's highest point, shown in Figure S1, Supporting Information) and have a web-like structure. It is apparent from the AFM image in Figure 2a that the i-SWNT film is composed of two distinct types of nanotube morphologies: wide bundles of nanotubes interwoven with a network of thin (or individual) tubes. Figure 2b is a magnified area of Figure 2a, showing the narrower tube features interspersed among the heavily bundled tubes. Wang et al. recently reported that bundled nanotubes are preferentially trapped at the organic−aqueous interface.[37] It is not clear here whether in this interfacial assembly process the bundled nanotubes will be aggregated first at the interface, followed by aggregation of the thinner and/or individual tubes or if the two structures are codeposited at the interface or from smaller clusters formed in solution after the addition of the antisolvent (ethanol) and before migration to the liquid−liquid interface. Nevertheless, it is believed that the electrical properties of these films are expected to be affected by this dual morphology structure.

Given the limitations of drop-casting, comparative samples were prepared by drop-casting of SWNT onto the substrates and their properties compared to those devices assembled from i-SWNT networks. It appears to be more difficult to control the thickness and the homogeneity of dc-SWNT films than by interfacial self-assembly. Most importantly, AFM and SEM images of dc-SWNT films (Figure 3a,b) showed that most nanotubes remain within thick bundles when directly deposited from the suspension to substrate. Electrical measurements of the i-SWNT film mounted on a Si bottom-gate substrate (SiO_2/Si) show that contact between Au electrodes and the film is ohmic and that the film is metallic in nature (i.e., shows no gate dependence). Table 1 shows a list of measured sheet resistance for drop-cast and interfacial films. It is believed that the significantly different film morphology will have a clear and pronounced effect on their functional properties. It is thought that if multiple layers of the i-SWNT film were layered onto a single sample it may be possible to decrease the sheet resistance to a value comparable with that for a dc-SWNT film. However, as the principal reason for using the interfacial films is to produce a thinner, optimized film (as discussed above) this is not necessary. It is noted that the quality of the films prepared by the drop-cast method strongly depends on the hydrophilicity of the substrates. For example, dc-SWNT films are inhomogeneous when deposited onto a hydrophobic surface. By contrast, thin and homogeneous i-SWNT films can be easily transferred on to either hydrophobic or hydrophilic substrates.

It has been noticed that the SiO_2/Si substrate can absorb photons and generate a photovoltage that may complicate the photoresponse of the devices.[38] It is important, therefore, to consider the photoresponse from the i-SWNT films on quartz.[39] Figure 4a shows that a reduction in drain current (I_d) is observed when an i-SWNT film is irradiated with light of wavelength 450 nm ($\sim 1.8 \times 10^{-2}$ W/cm^2). The bias applied between the source and drain (V_d) is 1 V for all photoresponse measurements.

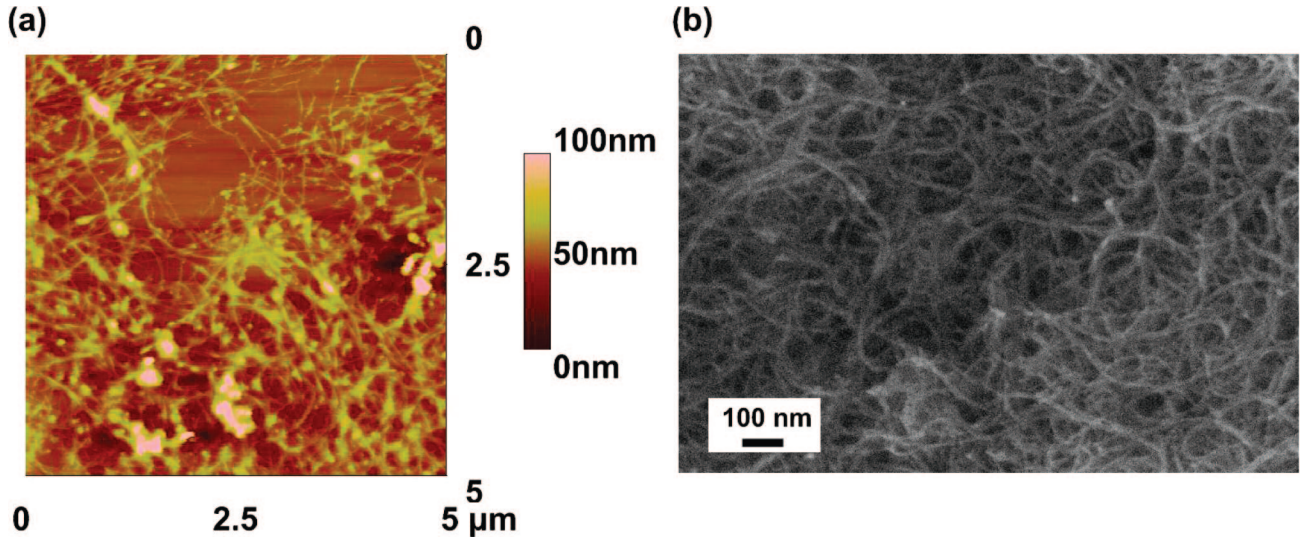

Figure 3. (a) AFM image of the dc-SWNT network on a quartz wafer. (b) SEM image of the sample in panel a showing aggregated and inhomogeneous structure (average thickness of the sample is around 80 nm).

TABLE 1: Summary of Electrical Characterization

	average thickness/nm	sheet resistance/kΩ^{-1}
i-SWNT film	25.2	20.1− 22.2
dc-SWNT1[a]	335.2[b]	0.563
dc-SWNT2[a]	372.0[b]	0.178
dc-SWNT3[a]	410.2[b]	0.137

[a] dc-SWNT1, dc-SWNT2, and dc-SWNT3 are three films prepared separately. [b] Drop-cast methods result in inhomogeneous, discontinuous films on quartz substrates, thus sheet resistance data are only available for films thicker than 300 nm where the 4-point probe measurement is possible.

The negative photocurrent has been attributed to the photodesorption of oxygen[28] for both individual SWNT and SWNT network devices. Further evidence for this is that the decrease in I_d becomes more significant if the i-SWNT device is exposed to a higher intensity UV light source (Xe arc lamp, ~200 W/cm^2) as shown in Figure 4a. This oxygen desorption phenomenon is manifest as a decreased photocurrent and as a negative slope in I_d profiles.

Fluorene-based polymers have been recently reported to interact strongly with carbon nanotubes[40] and thus the effect of addition of such polymers to the i-SWNT films was investigated. The photosensitive polymer poly[(9,9-dioctylfluorenyl-2,7-diyl)-co-(bithiophene)] (F8T2) was chosen because it was relatively stable in ambient conditions. Exciton diffusion lengths in conjugated polymers are typically very short (only tens of nanometers) and, as a consequence, the photoconductivity of a F8T2 polymer film in the absence of nanotubes was found to be undetectable when the channel length is relatively large (125 μm). The sheet resistance of the dc-SWNT and i-SWNT films are included in Table 1 above and the typical I_d-drain voltage (V_d) curve is included in the Supporting Information (Figure S2). Contrary to the decrease in photocurrent observed for the control film, an enhancement in photoresponse is observed for a composite i-SWNT film with a thin layer of F8T2 coated upon it (F8T2−i-SWNT). Figure 4b shows the I_d response for such a device under exposure to an ON-OFF cycle (λ = 450 nm, 1.8 × 10^{-2} W/cm^2). A decrease in I_d is seen within the first 25 s of the first ON phase; however, the I_d starts to increase during the second half of this phase. This suggests that although the O_2 desorption process is still occurring, the charge injection into the nanotubes from the photosensitive polymer is now

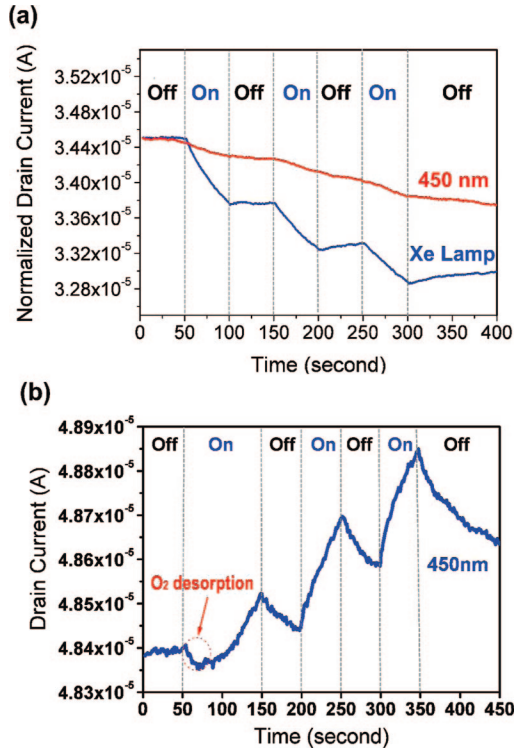

Figure 4. (a) A reduction in drain current (I_d) is observed when a light (λ = 450 nm, ~1.8 × 10^{-2} W/cm^2) is incident on the bare resistor device (top curve, red line). A more significant I_d reduction is seen (bottom curve, blue line) when exposed to a Xe light beam (~200 W/cm^2). (b) I_d response for a F8T2 coated i-SWNT network device (λ = 450 nm, ~1.8 × 10^{-2} W/cm^2). A decrease in I_d is seen in the first 25 s of the 1st ON cycle. The applied drain voltage (V_d) is 1 V.

competing with the O_2 desorption process, leading to a net positive photoresponse. It is possible that the presence of the polymer film acts to prevent readsorption of oxygen; however, the permeability of the polymer film, with regards to the extent to which oxygen can diffuse through the film, was not determined. It is believed, however, that this effect, if present, will be small enough to be negligible and indeed it was seen that for all subsequent cycles of illumination the oxygen desorption was not detectable.

Figure 5 illustrates the wavelength dependence of the I_d increase in F8T2−i-SWNT composite film, at a similar incident

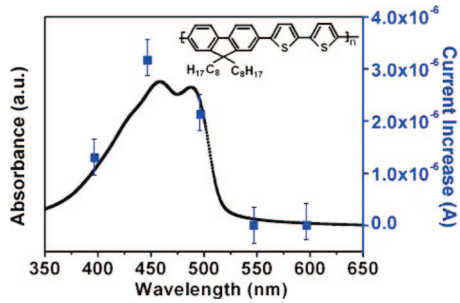

Figure 5. The wavelength dependence of the photocurrent generated in F8T2−SWNT as a function of wavelength of light (power intensity of 1.8×10^{-2} W/cm^2; spot size 125 μm).

power intensity of 1.8×10^{-2} W/cm^2 at different wavelength, where the I_d curves for extraction are the scans after eliminating the oxygen desorption effect. Optical absorption features of a pure F8T2 film are well correlated to the magnitude of the observed photocurrent of the F8T2−i-SWNT at several key wavelengths (Figure S3 in the Supporting Information shows how the photocurrent is calculated), confirming that the photoresponse results from the optical absorption of the F8T2 polymer coating. It can thus be concluded that these composite devices operate through a different mechanism than bare i-SWNT optical devices, which relied on the band absorption of semiconducting nanotubes or on the photodesorption of molecular species. The observation is consistent with previous reports on polymer-coated SWNT field effect transistors[32,33] where the nature of the photosensitive polymer governs the photoresponse.

A set of control experiments were performed in order to understand the nature of the photoresponse in the F8T2−i-SWNT system. To evaluate the importance of the structure of thin interfacial films of i-SWNT, the same SWNT aqueous solution used for the fabrication of i-SWNT films was deposited directly onto the solid substrates by drop casting. The composites of dc-SWNT films with F8T2 showed no measurable photocurrent. This may be related to the formation of a large number of bundled tubes (not contributing to the photoresponse) in the drop-cast samples. Photoresponse is suppressed by recombination in metallic nanotubes, and given that bundles are likely to contain metallic nanotubes this will suppress any photoresponse in the bundle as a whole. Given the inhomogeneity and extensive aggregation into bundles in drop-cast devices, the structure may be detrimental to net photocurrent generation due to the high probability that the carriers will recombine.

In addition, SWNT in our experiments were substituted with thin MWNT (outer diameter ~10 nm). Films of MWNT can also be assembled on a liquid−liquid interface by using the same conditions as those used for SWNT (Figure S4, Supporting Information), but again, as for dc-SWNT, i-MWNT films showed no photoresponsive behavior in polymer composites. This can be attributed to the fact that MWNT have truly metallic characteristics and, therefore, their composites with F8T2 cannot generate photocurrent. These control experiments clearly illustrate that the photoresponse in nanotube−polymer systems depends critically on the nature of nanotubes as well as on their morphology.

Previously we have suggested that quartz substrates, relative to SiO_2, minimize the electron trapping on surfaces, which allows us to observe intrinsic photointeraction between polymers and SWNT.[39] With no gate voltage applied, semiconducting SWNT operate at the accumulation mode and the majority of the carriers are holes. The observed I_d increase in F8T2-coated

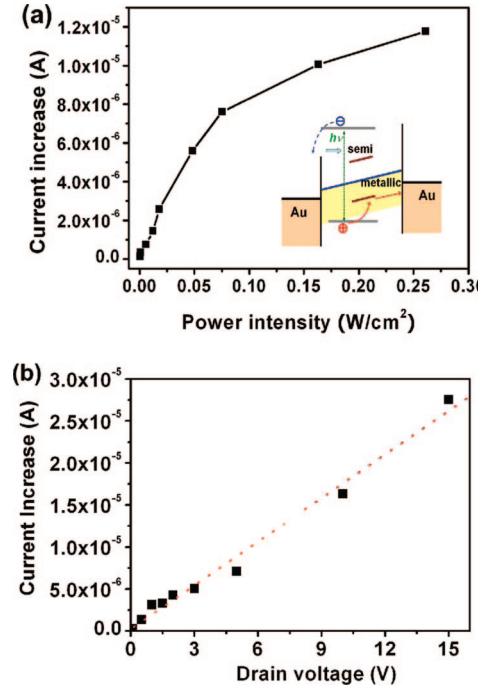

Figure 6. (a) The dependence of photocurrent on incident light intensity (λ = 450 nm). The inset shows the proposed band diagram and photocarrier flow. (b) The dependence of photocurrent on source-drain bias (under light power intensity of 1.8×10^{-2} W/cm^2; spot size 125 μm).

nanotube networks is simply because additional (photogenerated) holes are transferred from F8T2 to SWNT.[39,41] The proposed carrier path and band diagrams are illustrated in an inset of Figure 6a. The photoinduced excitons dissociate into electrons and holes at the F8T2−semiconducting SWNT interface,[42] where the holes are preferentially transferred to SWNT and electrons remain within the F8T2 polymer bands. The electric field built up by the applied bias drives the separated carriers to opposing electrodes and contributes to the photoresponse. In addition to the proposed mechanism (direct charge transfer) described, another possible mechanism could also contribute to the photoresponse: charge trapped within bundles of SWNT, or possibly at the functional groups (−COOH), may show effective gating[33] and thus contribute to the observed photoresponse. This requires further verification.

Panels a and b of Figure 6 show the photocurrent dependence on the light power and source drain bias (V_d), respectively. The photocurrent increases linearly with the incident light power (λ = 450 nm) when the light intensity is below 7.5×10^{-2} W/cm^2, indicating that this simple system can be used as a photodetector. When the light intensity is above 7.5×10^{-2} W/cm^2, the photocurrent approaches saturation. The linear dependence of photocurrent on V_d indicates that the photoresponse is strongly dependent on the drift velocity of the photogenerated carriers. It requires further study to understand whether the injection of carriers (electrons from F8T2 to Au electrode or holes from semiconducting to metallic nanotubes or Au electrodes) is another factor contributing to the photoresponse.

Conclusions

In summary, interfacial assembly of SWNT thin films allows the production of novel photoresponsive devices which, critically, are not possible to assemble with drop-casting techniques. A clear photoresponse is observed and the wavelength-dependent magnitude of this response can be directly correlated with

the absorbance of a photosensitive polymer coating. Thus charge transfer between the two components must occur with the nanotubes accepting photogenerated holes formed by exciton dissociation at the polymer−semiconducting SWNT interface. The interfacial SWNT films show metallic behavior in transfer curve (I_d versus gate voltage) measurements. The i-SWNT films consist of a robust interwoven mixture of thin and/or individual tubes which are easily transfer printed onto flexible PET substrates where they exhibit similar photoconductivity, suggesting that the nature of the substrates does not affect photoactivated charge transfer in the i-SWNT system. This study promises a simple and cost-effective approach for the fabrication of flexible photodetectors based on carbon nanotubes.

Acknowledgment. We acknowledge with thanks the support from Nanyang Technological University (Singapore) RG32/06 and MINDEF fund. A.N.K. thanks the European Science Foundation and the Royal Society.

Supporting Information Available: Figures showing the thickness of an i-SWNT film determined from the *z*-scale on the AFM images between the substrate and the film's highest point (Figure S1), typical drain current versus drain voltage characteristics of i-SWNT films (Figure S2), the method of extracting the photocurrent from I_d vs time measurement (Figure S3), and AFM image of a resistor device composed of an i-MWNT film (Figure S4). This material is available free of charge via the Internet at http://pubs.acs.org.

References and Notes

(1) Tan, S. J.; Verschueren, A. R. M.; Dekker, C. *Nature* **1998**, *393*, 49–52.
(2) Martel, R.; Schmidt, T.; Shea, H. R.; Hertel, T.; Avouris, Ph. *Appl. Phys. Lett.* **1998**, *73*, 2447–2449.
(3) Fuhrer, M. S.; Kim, B. M.; Durkop, T.; Brintlinger, T. *Nano Lett.* **2002**, *2*, 755–759.
(4) Radosavljevic, M.; Freitag, M.; Thadani, K. V.; Johnson, A. T. *Nano Lett.* **2002**, *2*, 761–764.
(5) Kong, J.; Franklin, N. R.; Zhou, C.; Chapline, M. G.; Peng, S.; Cho, K.; Dai, H. *Science* **2000**, *287*, 622–625.
(6) Star, A.; Gabriel, J. C. P.; Bradley, K.; Gruner, G. *Nano Lett.* **2003**, *3*, 459–463.
(7) Snow, E.; Perkins, F.; Houser, E.; Badescu, S.; Reinecke, T. *Science* **2005**, *307*, 1942–1945.
(8) Fu, D.; Lim, H.; Shi, Y.; Dong, X.; Mhaisalkar, S.; Chen, Y.; Moochhala, S.; Li, L. J. *J. Phys. Chem. C* **2008**, *112* (3), 650–653.
(9) Dong, X.; Fu, D.; Ahmed, M. O.; Shi, Y.; Mhaisalkar, S.; Zhang, S.; Ho, X.; Rogers, J. A.; Li, L. J. *Chem. Mater.* **2007**, *19*, 6059–6061.
(10) Gui, E. L.; Li, L. J.; Zhang, K.; Xu, Y.; Dong, X.; Ho, X.; Lee, P. S.; Kasim, J.; Shen, Z. X.; Rogers, J. A.; Mhaisalkar, S. *J. Am. Chem. Soc.* **2007**, *129*, 14427–14432.
(11) Lee, C.; Zhang, K.; Tantang, H.; Lohani, A.; Nagahiro, T.; Tamada, K.; Chen, Y.; Mhaisalkar, S. G.; Li, L. J. *Appl. Phys. Lett.* **2007**, *91*, 103515/1–103515/3.
(12) Snow, E. S.; Novak, J. P.; Campbell, P. M.; Park, D. *Appl. Phys. Lett.* **2003**, *82*, 2145–2147.
(13) Star, A.; Tu, E.; Niemann, J.; Gabriel, J. C. P.; Joiner, C. S.; Valcke, C. *Proc. Natl. Acad. Sci. U.S.A.* **2006**, *103*, 921–926.
(14) Hu, L.; Hecht, D. S.; Gruner, G. *Nano Lett.* **2004**, *4* (12), 2513–2517.
(15) Armitage, N. P.; Gabriel, J. C. P.; Grüner, G. *J. Appl. Phys.* **2003**, *95*, 3228–3230.
(16) Hecht, D. S.; Hu, L.; Grüner, G. *Appl. Phys. Lett.* **2006**, *89*, 133112/1–133112/3.
(17) Hecht, D. S.; Ramirez, R. A.; Artukovic, E.; Briman, M.; Chichak, K.; Stoddart, J. F.; Grüner, G. *Nano Lett.* **2006**, *6*, 2031.
(18) Fujitawa, A.; Matsuoka, Y.; Suematsu, H.; Ogawa, N.; Miyano, K.; Kataura, H.; Maniwa, Y.; Suzuki, S.; Achiba, Y. *Jap. J. Appl. Phys.* **2001**, *40*, L1229–L1231.
(19) Levitsky, I. A.; Euler, W. B. *Appl. Phys. Lett.* **2003**, *83*, 1857–1859.
(20) Freitag, M.; Martin, Y.; Misewich, J. A.; Martel, R.; Avouris, Ph. *Nano Lett.* **2003**, *3*, 1067–1071.
(21) Balasubramanian, K.; Fan, Y. W.; Burghard, M.; Kern, K.; Friedrich, M.; Wannek, U.; Mews, A. *Appl. Phys. Lett.* **2004**, *84*, 2400–2402.
(22) Stewart, D. A.; Leonard, F. *Nano Lett.* **2005**, *5*, 219–222.
(23) Balasubramanian, K.; Burghard, M. *Semicond. Sci. Technol.* **2006**, *21*, S22−S32.
(24) Balasubramanian, K.; Burghard, M.; Kern, K.; Scolari, M.; News, A. *Nano Lett.* **2005**, *5*, 507–510.
(25) Wei, J. Q.; Sun, J. L.; Zhu, J. L.; Wang, K. L.; Wang, Z. C.; Luo, J. B.; Wu, D. H.; Cao, A. Y. *Small* **2006**, *8*−*9*, 988–993.
(26) Lien, D. H.; Hsu, W. K.; Zan, H. W.; Tai, N. H.; Tsai, C. H. *Adv. Mater.* **2006**, *18*, 98–103.
(27) Lu, S.; Panchapakesan, B. *Nanotechnology* **2006**, *17*, 1843–1850.
(28) Che, R. J.; Franklin, N. R.; Kong, J.; Cao, J.; Tombler, T. W.; Zhang, Y.; Dai, H. *Appl. Phys. Lett.* **2001**, *79*, 2258–2260.
(29) Zhao, J.; Han, J.; Lu, J. P. *Phys. Rev. B* **2002**, *65*, 193401/1–193401/3.
(30) Shim, M.; Back, J. H.; Ozel, T.; Kwon, K. W. *Phys. Rev. B* **2005**, *71*, 205411/1–205411/7.
(31) Shim, M.; Giles, P. S. *Appl. Phys. Lett.* **2003**, *83*, 3564–3566.
(32) Star, A.; Lu, Y.; Bradley, K.; Gruner, G. *Nano Lett.* **2004**, *4*, 1587–1591.
(33) Borghetti, J.; Borghetti, J.; Derycke, V.; Lenfant, S.; Chenevier, P.; Filoramo, A.; Goffman, M.; Vuillaume, D.; Bourgoin, J.-P. *Adv. Mater.* **2006**, *18*, 2535–2540.
(34) Li, Y. F.; Kaneko, T.; Hatakeyama, R. *Appl. Phys. Lett.* **2008**, *92*, 183115–183117.
(35) Marsh, D. H.; Rance, G. A.; Whitby, R. J.; Giustiniano, F.; Khlobystov, A. N. *J. Mater. Chem.* **2008**, *18*, 2249–2256.
(36) Marsh, D. H.; Rance, G. A.; Zaka, M. H.; Whitby, R. J.; Khlobystov, A. N. *Phys. Chem. Chem. Phys.* **2007**, *9*, 5490–5496.
(37) Wang, R. K.; Reeves, R. D.; Ziegler, K. *J. Am. Chem. Soc.* **2007**, *129* (14), 15124–15125.
(38) Marcus, M. S.; Simmons, J. M.; Castellini, O. M.; Hamers, R. J.; Eriksson, M. A. *J. Appl. Phys.* **2006**, *100*, 084306/1–084306/6.
(39) Shi, Y.; Tantang, H.; Lee, C. W.; Weng, C.-H.; Dong, X.; Li, L. J.; Chen, P. *Appl. Phys. Lett.* **2008**, *92*, 103310/1–103310/3.
(40) Chen, F.; Wang, B.; Chen, Y.; Li, L. J. *Nano Lett.* **2007**, *7*, 3013–3017.
(41) Chawla, S.; Gupta, D.; Narayan, K. S.; Zhang, R. *Appl. Phys. Lett.* **2007**, *91*, 043510/1–043510/3.
(42) Yang, C.; Wohlgenannt, M.; Vardeny, Z. V.; Blau, W. J.; Dalton, A. B.; Baughman, R.; Zakhidov, A. A. *Phys. B* **2003**, *338*, 366–369.

JP803477T